



HAL
open science

Enhancement of iron-mediated activation of persulfate using catechin: From generation of reactive species to atenolol degradation in water

Yanlin Wu, Olivier Monfort, Wenbo Dong, Marcello Brigante, Gilles Mailhot

► To cite this version:

Yanlin Wu, Olivier Monfort, Wenbo Dong, Marcello Brigante, Gilles Mailhot. Enhancement of iron-mediated activation of persulfate using catechin: From generation of reactive species to atenolol degradation in water. *Science of the Total Environment*, 2019, 697, pp.134188. 10.1016/j.scitotenv.2019.134188 . hal-02470622

HAL Id: hal-02470622

<https://hal.science/hal-02470622>

Submitted on 9 Dec 2020

HAL is a multi-disciplinary open access archive for the deposit and dissemination of scientific research documents, whether they are published or not. The documents may come from teaching and research institutions in France or abroad, or from public or private research centers.

L'archive ouverte pluridisciplinaire **HAL**, est destinée au dépôt et à la diffusion de documents scientifiques de niveau recherche, publiés ou non, émanant des établissements d'enseignement et de recherche français ou étrangers, des laboratoires publics ou privés.

1 **Enhancement of iron-mediated activation of persulfate using catechin:** 2 **from generation of reactive species to atenolol degradation in water**

3
4 Yanlin Wu^{a,b,c}, Olivier Monfort^b, Wenbo Dong^{a,c}, Marcello Brigante^{b*}, Gilles Mailhot^b

5
6 ^aShanghai Key Laboratory of Atmospheric Particle Pollution and Prevention, Department of Environmental Science &
7 Engineering, Fudan University, Shanghai 200433, China

8 ^bUniversité Clermont Auvergne, CNRS, SIGMA Clermont, Institut de Chimie de Clermont-Ferrand, F-63000
9 Clermont-Ferrand, France

10 ^cShanghai institute of pollution control and ecological security, Shanghai 200092, China

11 *marcello.brigante@uca.fr ; 24 avenue Blaise Pascal, 63178 Aubière Cedex, France

14 **Abstract**

15 Persulfate (PS) activation reaction, which forms sulfate radical ($\text{SO}_4^{\bullet-}$), can be used to degrade
16 organic pollutants in water. However, a drawback of this reaction is that the regeneration of
17 ferrous ions requires a high concentration of hydrogen peroxide (Fenton-like reaction) or use of
18 UV radiation. Catechin (CAT), a non-toxic antioxidant of natural origin from tea, is used in this
19 work to improve the sulfate radical-mediated degradation of atenolol (ATL, a model pollutant) in
20 water using relatively low concentrations of reactive chemical species (less than 100 μM).

21 To the best of the author's knowledge, the direct effect of CAT on the oxidation state of iron,
22 which is promoted by the reduction of ferric into ferrous ions with the enhancement of $\text{SO}_4^{\bullet-}$
23 formation in the presence of PS, is demonstrated for the first time. The enhancement versus
24 inhibition effect of CAT and the chemical mechanism of the iron-based activation process are
25 explained. Results show that UVA radiation, which is representative of solar light, accelerates the

26 initial degradation of ATL by more than 30% through ferric iron photolysis. Finally, a reaction
27 mechanism leading to the formation of hydroxyl radicals (HO^\bullet) and $\text{SO}_4^{\bullet-}$ is proposed considering
28 the implication of different activation/reaction chemical steps.

29

30 **Keywords:** Pollutant degradation, sulfate radical, hydroxyl radical, iron reduction

31

32 **Highlights**

- 33 • Catechin efficiently reduced ferric to ferrous ions in water
- 34 • The positive versus negative effect of CAT on the persulfate activation was assessed
- 35 • The degradation of atenolol was strongly improved in the presence of CAT
- 36 • A reaction mechanism considering the involvement of radical species was proposed

37

38 **1. Introduction**

39 The Fenton process based on the Fe(II/III) redox cycle in the presence of hydrogen peroxide
40 was described for the first time in 1894 (Fenton, 1894) and has been used for the degradation of a
41 wide range of organic contaminants. In the last decades, many works focusing on the modified
42 Fenton-like process have been proposed to stabilize and generate additional Fe(II) species and
43 improve the removal efficiency of organic contaminants in water (Kaur et al., 2019; Li et al., 2016;
44 Romero et al., 2016; Tian et al., 2017). These modified reactions, such as ferric ion (Fe(III))
45 photoreduction or complexation with organic ligands, have also been used for persulfate (PS)
46 activation to generate additional Fe(II) and sulfate radical ($\text{SO}_4^{\bullet-}$) (Bi et al., 2016; Jiang et al.,
47 2017; Wu et al., 2015). Furthermore, the reaction mechanism was becoming increasingly clear,
48 and the concentration of ferrous iron in water was found to be the most critical parameter.

49 Therefore, researchers investigated different technologies, such as reaction in acidic media (Velo
50 Gala et al., 2014), use of irradiation (Giannakis et al., 2018; Hinojosa Guerra et al., 2019),
51 presence of organic ligands (De Luca et al., 2015; Huang et al., 2013; Wang et al., 2019), and
52 reduction conditions (Nazari et al., 2018; Wu et al., 2016), to enhance the Fe(II)
53 formation/regeneration.

54 Antioxidant agents, such as polyphenolic compounds, are known for their anti-aging,
55 anti-carcinogenic, and anti-atherosclerotic properties (Brown et al., 2011). Green tea is rich in
56 polyphenolic compounds, especially (+)-catechin (CAT) (Yang et al., 2018). CAT has catecholate
57 groups that easily chelate Fe^{3+} , which makes it susceptible to undergo light-induced ligand
58 oxidation and Fe^{3+} reduction (Barbeau, 2006; Barbeau et al., 2001). Dong et al. already used
59 another polyphenolic compound (gallic acid), which played an important role on Fe(II)
60 formation/regeneration and promoted the efficiency of $\text{H}_2\text{O}_2/\text{Fe(III)}$ system in the degradation of
61 methyl orange (Dong et al., 2016). However, we believe that studies assessing the mechanism of
62 radical generation and reactivity through iron reduction have not been reported.

63 Atenolol (ATL), a widely used pharmaceutical which exhibits toxicity on freshwater species and
64 inhibition on human embryonic cell growth, was selected as the target pollutant (de Jesus Gaffney
65 et al., 2015). ATL is also considered a recalcitrant pollutant due to its slow biodegradation and
66 high persistence under sunlight in water (Yamamoto et al., 2009). Under chlorination or UV
67 treatment, ATL leads to the fast formation of products with high toxicity in water (DellaGreca et
68 al., 2009; Diniz et al., 2015).

69 In the present work, the mechanism of $\text{SO}_4^{\bullet-}$ generation in the Fe(III)/PS system, as well as
70 the formation of Fe(II) and ATL degradation, was investigated for the first time using CAT.

71 Interestingly, as a non-toxic extract from green tea, CAT shows high stability and solubility in
72 water, which makes it a good candidate for contaminant removal application. The effect of CAT,
73 Fe(III), and PS concentrations on the degradation efficiency of ATL was also studied, and the role
74 of oxidative radicals as well as the second-order reaction rate constants with generated radicals
75 ($\text{HO}^\bullet/\text{SO}_4^{\bullet-}$) was elucidated. An activation and reactivity system, in which CAT plays a key role,
76 was proposed to assess the enhancement versus inhibition role of antioxidant agents as reduction
77 species for iron but also as radical scavengers in water. Finally, the effect of solar spectrum UVA
78 radiation on the CAT-mediated persulfate activation system was evaluated.

79

80 **2. Materials and methods**

81 *2.1 Chemicals*

82 Sodium persulfate ($\text{Na}_2\text{S}_2\text{O}_8$, PS), Atenolol (ATL), (+)-catechin (CAT), Ferrozine, isopropanol
83 (2-Pr), and tert-Butanol (t-BuOH) were obtained from Sigma-Aldrich. Ferric perchlorate
84 ($\text{Fe}(\text{ClO}_4)_3$) was obtained from Fluka. Perchloric acid (HClO_4) and sodium hydroxide were used to
85 adjust the pH of the solutions. All chemicals were utilized without further purification. All
86 solutions were prepared in milli-Q water (18.2 M Ω cm). Unless otherwise stated, all experiments
87 were performed at pH 3.3 to maintain soluble iron in water (homogeneous reactivity).

88

89 *2.2 Experimental Procedure*

90 All experiments in the absence of light (dark) were conducted in a brown bottle at ambient
91 temperature (298 ± 2 K). A total of 50 mL mixture was magnetically stirred during the reaction,
92 and samples were withdrawn at fixed intervals. The samples were then analyzed using UV-vis

93 spectroscopy and high-performance liquid chromatography (HPLC-UV) (section 2.3). A total of
94 10 μM of ATL was used in all the experiments. The effect of different concentrations of CAT, PS,
95 and iron was investigated at pH approximately 3.3. Irradiation experiments were conducted in a
96 homemade photoreactor equipped with four UVA lamps (TLD 15W/05, Philips, Netherlands)
97 located on the top of the solution. The emission spectrum of the lamp is shown in Fig. S1.

98

99 *2.3 Quantitative analysis of ATL and iron*

100 The ATL concentration in the samples was determined using ultra-performance liquid
101 chromatography (UPLC) (Waters, USA) with C18 column (BEH, 100 mm \times 2.1 mm \times 1.7 μm),
102 and the mobile phase was an ammonium acetate (0.01 M)/methanol solution with 70:30 (v/v). The
103 flow rate was 0.25 mLmin⁻¹, and the detection wavelength was 224 nm. The CAT concentration
104 was determined by HPLC (Waters, USA) with C18 column (Agilent, 250 mm \times 4.6 mm \times 5 μm),
105 and the mobile phase was an acetonitrile/formic acid (0.5%) solution with 25:75 (v/v). The flow
106 rate was 0.6 mL min⁻¹, and the detection wavelength was 279 nm. Fe(II) was quantified using a
107 colorimetric method based on ferrozine complexation (Stookey, 1970).

108

109 *2.4 Second-order kinetic constants determination*

110 Two different methods were used to determine the second-order rate constant of ATL and CAT
111 with sulfate and hydroxyl radicals ($\text{SO}_4^{\bullet-}$ and HO^\bullet), respectively. For HO^\bullet , the transient absorption
112 spectroscopy was adopted to investigate the reactivity with CAT and ATL. In this approach, a laser
113 flash photolysis (LFP) system using an excitation wavelength of 266 nm coupled with UV-vis
114 detection could follow the radical absorption signal decay or its formation in the presence of

115 different CAT and ATL concentrations. Similar experimental procedures and conditions were
116 already detailed in previous works, and only a brief description is provided in the SM section
117 (Huang et al., 2018; Wu et al., 2015).

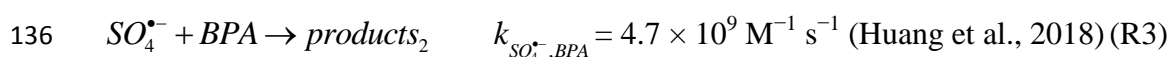
118 For the reactivity between $SO_4^{\bullet-}$ and ATL, the formation of a new transient species absorbed
119 around 450 nm close to the signal of $SO_4^{\bullet-}$ interfered with the kinetic decay (Fig. S2). Hence, a
120 different method using a competition kinetic approach under steady-state irradiation (UVA) in the
121 presence of Bisphenol A (BPA) was used to determine the reactivity constant between $SO_4^{\bullet-}$ and
122 ATL. Meanwhile, the reactivity constant between $SO_4^{\bullet-}$ and CAT of the transient-state absorption
123 of $SO_4^{\bullet-}$ could be directly investigated.

124

125 **3. Results and discussion**

126 *3.1 Reactivity of hydroxyl and sulfate radicals with ATL and CAT*

127 The reactivity between ATL and CAT with generated radicals ($SO_4^{\bullet-}/HO^{\bullet}$) was determined to
128 assess the effect of different reaction pathways during the Fenton-like reaction. For the reactivity
129 between $SO_4^{\bullet-}$ and CAT, a solution containing 10 mM of PS was used to generate $SO_4^{\bullet-}$ under
130 UVA irradiation (R1). BPA was used as a reference compound, and no direct photolysis under
131 UVA irradiation was observed (Huang et al., 2018). A competition kinetic approach considering
132 the decays of ATL and BPA concentrations during times (R2 and R3) was used to determine the
133 second-order rate constant (R2 and R3) following Eq. 1.



137 The competition kinetic reaction gives:

138
$$\ln \frac{[ATL]_0}{[ATL]_t} = \frac{k_{SO_4^{\cdot-}, ATL}}{k_{BPA, ATL}} \ln \frac{[BPA]_0}{[BPA]_t}, \quad (\text{Eq1})$$

139 where $[ATL]_0$ and $[BPA]_0$ were the initial concentrations (25 μM), and $[ATL]_t$ and $[BPA]_t$ were the

140 remaining concentrations at time t . The slope of the linear fit of $\ln[ATL]_0/[ATL]_t$ versus

141 $\ln[BPA]_0/[BPA]_t$ provided the second-order rate constant $k_{SO_4^{\cdot-}, ATL} = (1.65 \pm 0.25) \times 10^9 \text{ M}^{-1} \text{ s}^{-1}$.

142 Other constants with HO^\bullet were determined using chemical competition reactivity in the presence

143 of thiocyanate anion (SCN^-), which led to the formation of di-thiocyanate radical anion ($\text{SCN}_2^{\cdot-}$)

144 followed at 470 nm using LFP experiments (see SM for experimental procedure and Fig. S3).

145 CAT was found to be approximately twice more reactive with $\text{SO}_4^{\cdot-}$ and HO^\bullet than ATL (Table 1).

146 The high reactivity of CAT toward electron transfer reaction (main reactive pathway of $\text{SO}_4^{\cdot-}$) is

147 attributed to the presence of two lone electron pairs on the phenolic groups. This high affinity with

148 radical species also suggests a possible scavenging effect of CAT (*i.e.*, negative contribution)

149 during the ATL degradation experiments.

150

151 3.2 Reactivity between Fe^{3+} and CAT

152 UV-vis spectroscopy was used to investigate the possible reactivity between CAT and ferric ions

153 (Fe^{3+}) in the solution. A total of 100 μM CAT solution was found to be stable in dark condition at

154 least five days. The spectroscopic analysis of solutions at different pH is presented in Fig. S4.

155 From pH 2.5 to 6.0, no significant differences in the UV-vis spectra of CAT were observed, and

156 the same absorption maximum at 279 nm was found ($\epsilon_{279} = (3610 \pm 70) \text{ M}^{-1} \text{ cm}^{-1}$). A

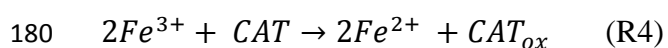
157 bathochromic shift (from 279 nm to 290 nm) was observed when the pH increased from 7.8 to

158 11.3, and a shoulder appeared at 320 nm at a high pH. This redshift corresponded to the

159 deprotonation of phenolic groups on CAT occurrence at high pH values (pKa approximately 9.0).
160 In the presence of 100 μM of CAT at pH 3.3, the UV-vis spectrum of 100 μM solution of ferric
161 ions was strongly modified (Fig. 1); no additional absorption was observed at wavelengths higher
162 than 300 nm. The UV-vis spectrum of the solution indicated the absence of CAT in the solution,
163 whereas no spectroscopic contribution of Fe^{3+} was observed. Moreover, the UV-vis spectrum of
164 solution demonstrated a slight bathochromic shift compared with that of pure CAT. This effect was
165 due to the possible electron transfer from the phenolic groups of CAT to Fe^{3+} , leading to the
166 formation of quinone groups as previously observed during selective oxidation of CAT (Tanaka
167 and Kouno, 2003). No significant differences between the spectra of Fe^{3+} and Fe^{2+} in the presence
168 of CAT were observed (Fig. 1 insert).

169 The concentration of Fe^{2+} in the solution was monitored during the mixture of 100 μM of Fe^{3+}
170 with different CAT concentrations to clarify the interaction mechanism between CAT and Fe^{3+} . As
171 reported in Figure 2A, the formation of a significant amount of Fe^{2+} from Fe^{3+} solution (100 μM)
172 was strongly correlated to the initial CAT concentration. The plot of ratios between $[\text{Fe}^{2+}]$ and
173 $[\text{Fe}_{\text{tot}}]$ as function of initial CAT/ Fe^{3+} concentrations ($[\text{CAT}]/[\text{Fe}^{3+}]$) reported in Figure 2B
174 indicated the significant formation of Fe^{2+} . Fe^{2+} immediately reached a plateau in all experiments.
175 This finding suggests that Fe^{3+} was quantitatively converted into Fe^{2+} following a reaction with a
176 stoichiometry (R4) of 1 mole of CAT with 2 moles of Fe^{3+} . To explain the ferrous ions generation,
177 we can consider that semiquinone and quinone (CAT_{ox}) might stepwise be formed with each step
178 being a single electron transfer from the two phenolic groups.

179



181

182 3.3 Effect of CAT on the modified PS activation process

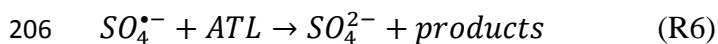
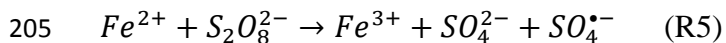
183 3.3.1 ATL degradation

184 The reactivity of CAT (5 μM) in the solution containing 50 and 100 μM of Fe^{3+} and PS,
185 respectively, was investigated by monitoring the degradation of ATL and the formation of Fe^{2+}
186 during the reaction (Fig. 3). No ATL degradation was observed after 60 min in blank experiments,
187 that is, using ATL + PS, ATL + Fe^{3+} , ATL + CAT, ATL + PS + CAT, and ATL + Fe^{3+} + CAT;
188 meanwhile, only 10% degradation could be determined in the system Fe^{3+} + PS (Fig. 3). However,
189 in Fe^{2+} + PS system, a fast ATL initial degradation rate (R_{ATL}^d) was observed during the first 10
190 min ($2.51 \pm 0.50 \times 10^{-7} \text{ M min}^{-1}$) and followed by a plateau. ATL (30%) was degraded in Fe^{2+} + PS
191 system after 60 min of reaction. This reactivity could be explained by considering the formation of
192 $\text{SO}_4^{\bullet-}$ through the well-known PS activation reaction (R5). The plateau was due to the fast
193 reactivity of Fe^{2+} in the system, while no additional Fe^{3+} could be converted back to Fe^{2+} without a
194 reducing agent. When 50 μM of Fe^{3+} was previously mixed with 5 and 100 μM of CAT and PS,
195 respectively, a similar trend was observed for the first 10 min ($R_{ATL}^d = 2.12 \pm 0.44 \times 10^{-7} \text{ M min}^{-1}$),
196 whereas ATL concentration continued to decrease by up to 52% of the initial concentration after
197 60 min (Fig. 3).

198 The enhancing effect observed in the presence of CAT could be explained by observing the Fe^{2+}
199 formation during the reaction (insert Fig. 3). As expected, approximately 10 μM of Fe^{2+} was
200 observed when 50 μM of Fe^{3+} was mixed with 5 μM of CAT (R4), and Fe^{2+} concentration
201 remained stable during its time in the ATL + Fe^{3+} + CAT system. However, when 100 μM of PS
202 was present in the solution (ATL + Fe^{3+} + CAT + PS), Fe^{2+} could activate PS for $\text{SO}_4^{\bullet-}$ formation

203 (R5), thereby leading to enhance ATL degradation (R6).

204



207

208 The higher efficiency in the presence of CAT/Fe³⁺/PS than that of Fe²⁺/PS highlighted the role of
209 CAT for the regeneration of Fe²⁺ during the process and its capability to activate the cycle between
210 Fe²⁺ and Fe³⁺.

211

212 3.3.2 Antagonist role of CAT and oxidant species occurrence

213 Although CAT could enhance SO₄^{•-} formation via Fe²⁺ generation, it could also scavenge
214 generated radicals (Table 1), thus partially inhibiting the ATL degradation. The stability of CAT in
215 the presence of Fe³⁺, ATL, and PS is reported in Figure 4A. No direct reaction between CAT and
216 ATL was observed. Meanwhile, slight CAT oxidation occurred in the presence of PS
217 (approximately 25% after 1 h). However, approximately 75% of CAT was degraded in the
218 presence of Fe³⁺ after 60 min (with a pseudo-first-order decay k' = 8.4 ± 1.3 × 10⁻² min⁻¹) due to
219 the oxidation corresponding to the formation of Fe²⁺ through electron transfer reaction (R4).
220 Complete degradation of CAT was achieved in the Fe³⁺+PS system after 10 min (k' = 2.7 ± 0.5 ×
221 10⁻¹ min⁻¹) due to the reaction of generated SO₄^{•-} with CAT. When ATL was observed in the Fe³⁺
222 + PS system, CAT degradation slightly decreased (k' = 2.3 ± 0.1 × 10⁻¹ min⁻¹) due to the
223 competitive reaction of SO₄^{•-} with ATL. Therefore, finding the optimal concentration of CAT for
224 efficient wastewater treatment and assessment of positive versus negative effect on modified

225 activation of PS is crucial.

226 ATL degradation was monitored using different CAT concentrations (from 0 to 25 μM) in the
227 presence of 50 μM of Fe^{3+} and 100 μM of PS (Fig. 4B). When the CAT concentration was raised
228 up to 5 μM , the pseudo-first-order decay of ATL (k'_{ATL}) increased by approximately two orders of
229 magnitude (from 2.3×10^{-3} to $1.6 \times 10^{-1} \text{ min}^{-1}$) (R5) through the formation of Fe^{2+} (R4) due to PS
230 activation. The ATL degradation rate at 60 min was enhanced from 10% to 52% with CAT
231 concentration up to 5 μM . When the CAT concentration was raised to 25 μM , the k'_{ATL} decreased
232 to $8.6 \times 10^{-3} \text{ min}^{-1}$, and ATL degradation rate decreased to 32%. This negative effect observed at
233 high CAT concentrations was attributed to the reactivity between CAT (or its oxidation products)
234 and $\text{SO}_4^{\bullet-}$, which competed with ATL degradation. Given the second-order rate constants reported
235 in Table 1, the initial ATL and CAT concentrations, and the similar reactivity of CAT oxidation
236 products (reasonably quinone derivatives), the $\text{SO}_4^{\bullet-}$ selectivity on each reactive species in
237 solution ($S_X^{\text{SO}_4^{\bullet-}}$ (%)) can be estimated as follows:

$$238 \quad S_X^{\text{SO}_4^{\bullet-}} (\%) = \frac{k''_{\text{SO}_4^{\bullet-}, X} \times [X]}{\sum_i k''_{\text{SO}_4^{\bullet-}, S_i} \times [S_i]} \times 100,$$

239 where $[X]$ was the initial concentration of reference compounds, and $k''_{\text{SO}_4^{\bullet-}, X}$ is the second-order
240 rate constant with $\text{SO}_4^{\bullet-}$. $\sum_i k''_{\text{SO}_4^{\bullet-}, S_i} \times [S_i]$ was calculated from the sum of the contribution of the
241 initial concentration of all reactive species in the solution (i.e., CAT, PS, and ATL) with the
242 second-order rate constant of $\text{SO}_4^{\bullet-}$.

243 Under adopted experimental conditions reported in Figure 4B, when CAT concentration was 5 μM ,
244 approximately 57% of $\text{SO}_4^{\bullet-}$ reacted with ATL while 43% reacted with CAT. However, in the
245 presence of 25 μM of CAT, only 21% of $\text{SO}_4^{\bullet-}$ reacted with ATL and up to 79% reacted with CAT.
246 In all experiments, less than 0.5% of $\text{SO}_4^{\bullet-}$ was scavenged by PS due to the low reactivity constant

247 $(k''_{SO_4^{\bullet-}, PS} = 1.2 \times 10^6 \text{ M}^{-1} \text{ s}^{-1})$ (Neta et al., 1988).

248

249 3.4 UVA effect on modified PS activation system

250 The effect of UVA irradiation on ATL degradation is reported in Figure 5 using different systems.

251 No ATL degradation was observed under UVA with or without CAT (blank experiments not

252 reported in Figure 5). However, approximately 10% and 35% of ATL degradation could be

253 achieved after 60 min using either 100 μM of PS or 50 μM of Fe^{3+} , respectively. This process

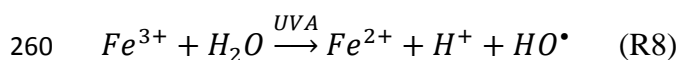
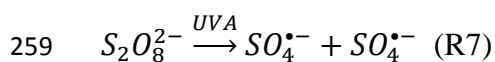
254 could be attributed to the UVA-mediated formation of $\text{SO}_4^{\bullet-}$ (PS photolysis) (R7) and HO^\bullet

255 (iron–aqua complex photolysis) (R8) in the solution. A redox cycle including HO^\bullet and $\text{SO}_4^{\bullet-}$

256 enhanced the ATL degradation with the presence of PS and Fe^{3+} in the solution. The ATL

257 degradation extent was increased from 52% to 80% in the presence of UVA in the system

258 containing 10 μM of ATL mixed with 5 μM of CAT, 50 μM of Fe^{3+} , and 100 μM of PS.



261

262 Thus, high efficiency was observed in the presence of light. This finding indicates the presence of

263 an important complementarity between the formation of Fe^{2+} through Fe^{3+} reduction by UVA

264 radiation and CAT.

265

266 3.5 Radical species involvement

267 Scavenging experiments were performed by using isopropanol (2-Pr) and tert-butanol (t-BuOH) to

268 assess the involvement of different radical species during ATL degradation in the presence of Fe^{3+}

269 and PS. Meanwhile, 2-Pr was used as a quencher of HO[•] and SO₄^{•-} ($k_{2\text{-Pr},\text{HO}^\bullet} = 1.9 \times 10^9 \text{ M}^{-1} \text{ s}^{-1}$,
270 $k_{2\text{-Pr},\text{SO}_4^{\bullet-}} = 6.9 \times 10^7 \text{ M}^{-1} \text{ s}^{-1}$), and t-BuOH selectively reacted with HO[•] rather than with SO₄^{•-} due
271 to differences between reactivity constants of the two radicals ($k_{\text{t-BuOH},\text{HO}^\bullet} = 6.0 \times 10^8 \text{ M}^{-1} \text{ s}^{-1}$ and
272 $k_{\text{t-BuOH},\text{SO}_4^{\bullet-}} = 8.4 \times 10^5 \text{ M}^{-1} \text{ s}^{-1}$) (Buxton et al., 1988; Neta et al., 1988). A concentration of 10 mM
273 of each scavenger was adopted to trap specific radical species (in the case of (t-BuOH) efficiently
274 also considering the possible competition effect of CAT in the solution.
275 The effect of 2-Pr and t-BuOH was compared when 10 μM of ATL was used in the presence of 5
276 μM of CAT, 50 μM of Fe³⁺, and 100 μM of PS at pH = 3.3. No significant difference in ATL
277 degradation was observed with t-BuOH (for both system k' approximately $1.2 \pm 0.1 \times 10^{-2} \text{ min}^{-1}$)
278 (Figure 6A). By contrast, the ATL degradation was completely inhibited using 2-Pr, indicating that
279 only SO₄^{•-} was generated under dark conditions. Under UVA irradiation (Fig. 6B), the ATL
280 degradation was partially inhibited with t-BuOH (k' without scavengers = $3.2 \pm 0.3 \times 10^{-2} \text{ min}^{-1}$
281 and k' with t-BuOH = $1.8 \pm 0.2 \times 10^{-2} \text{ min}^{-1}$). However, almost no degradation could be observed
282 in the presence of 2-Pr. Considering the reactivity constants of radical with ATL and scavengers,
283 approximately 77% and 23% of ATL degradation under UVA were attributed to SO₄^{•-} and HO[•],
284 respectively. The generation of the two radicals was considered an asset for the degradation of
285 water containing different kind of pollutants.

286

287 **4. Conclusions**

288 Ferrous iron was the key parameter in PS activation processes, and many efforts have been made
289 in the direction of formation/regeneration of reactive species under different conditions. For the
290 first time, the present work investigated the use of CAT, a non-toxic and natural antioxidant, on the

291 reduction capability of Fe^{3+} into Fe^{2+} in a modified PS activation process ($\text{Fe}^{3+}/\text{CAT}/\text{PS}$).

292 An optimal concentration of CAT (5 μM) was utilized for systems containing 50 μM of Fe^{3+} and

293 100 μM of PS to limit the competitive reaction with generated radicals and target pollutant (ATL).

294 Under such low concentration conditions, the high degradation extent of 10 μM ATL could be

295 achieved in the dark after 60 min (approximately 50%). CAT was complementary to PS in the

296 reduction/oxidation cycle of $\text{Fe(III)}/\text{Fe(II)}$. Under UVA irradiation, the modified PS activation

297 process was enhanced and reached almost 80% of ATL degradation. Moreover, the only reactive

298 species involved in the dark conditions was the $\text{SO}_4^{\cdot-}$. Meanwhile, HO^{\cdot} also contributed up to

299 approximately 25% of the total radical generation under UVA. Moreover, products from waste

300 green tea leaves were proven useful in Fe(III) reduction to produce Fe(II) . This work strengthened

301 the possible use of waste (tea leaves) for water application treatments.

302
303
304

305 **ACKNOWLEDGMENTS**

306 Authors acknowledge financial support from National Natural Science Foundation of China

307 (NSFC 21607116), the Region Council of Auvergne Rhône Alpes, and the “Fédération des

308 Recherches en Environnement” through the CPER “Environment” founded by the Region AURA,

309 the French government, the FEDER from the European Community and PRC program

310 CNRS/NSFC n°270437, and the CAP 20-25 I-site project.

311

312 **References**

- 313 Barbeau K., 2006. Photochemistry of organic iron(III) complexing ligands in oceanic systems. *Photochem. Photobiol.*
314 82, 1505-1516.
- 315 Barbeau K., Rue E.L., Bruland K.W., Butler A., 2001. Photochemical cycling of iron in the surface ocean mediated by
316 microbial iron(III)-binding ligands. *Nature* 413, 409-413.
- 317 Bi W., Wu Y., Wang X., Zhai P., Dong W., 2016. Degradation of oxytetracycline with SO_4^- under simulated solar light.
318 *Chem. Eng. J.* 302, 811-818.
- 319 Brown A.L., Lane J., Holyoak C., Nicol B., Mayes A.E., Dadd T., 2011. Health effects of green tea catechins in
320 overweight and obese men: a randomised controlled cross-over trial. *Br. J. Nutr.* 106, 1880-9.
- 321 Buxton G.V., Greenstock C.L., Helman W.P., Ross A.B., 1988. Critical review of rate constants for reactions of hydrated
322 electrons, hydrogen atoms and hydroxyl radicals ($^{\circ}\text{OH}/\text{O}^{\circ-}$) in aqueous solution. *J. Phys. Chem. Ref. Data* 17,
323 513-886.
- 324 de Jesus Gaffney V., Almeida C.M.M., Rodrigues A., Ferreira E., Benoliel M.J., Cardoso V.V., 2015. Occurrence of
325 pharmaceuticals in a water supply system and related human health risk assessment. *Water Res.* 72,
326 199-208.
- 327 De Luca A., Dantas R.F., Esplugas S., 2015. Study of Fe(III)-NTA chelates stability for applicability in photo-Fenton at
328 neutral pH. *Appl. Catal., B* 179, 372-379.
- 329 DellaGreca M., Iesce M.R., Pistillo P., Previtiera L., Temussi F., 2009. Unusual products of the aqueous chlorination of
330 atenolol. *Chemosphere* 74, 730-734.
- 331 Diniz M.S., Salgado R., Pereira V.J., Carvalho G., Oehmen A., Reis M.A.M., et al., 2015. Ecotoxicity of ketoprofen,
332 diclofenac, atenolol and their photolysis byproducts in zebrafish (*Danio rerio*). *Sci. Total Environ.* 505,
333 282-289.

334 Dong H., Sans C., Li W., Qiang Z., 2016. Promoted discoloration of methyl orange in H₂O₂/Fe(III) Fenton system:
335 Effects of gallic acid on iron cycling. *Sep. Purif. Technol.* 171, 144-150.

336 Fenton H.J.H., 1894. LXXIII.—Oxidation of tartaric acid in presence of iron. *J. Chem. Soc. Trans.* 65, 899-910.

337 Giannakis S., Le T.-T.M., Entenza J.M., Pulgarin C., 2018. Solar photo-Fenton disinfection of 11 antibiotic-resistant
338 bacteria (ARB) and elimination of representative AR genes. Evidence that antibiotic resistance does not
339 imply resistance to oxidative treatment. *Water Res.* 143, 334-345.

340 Hinojosa Guerra M.M., Oller Alberola I., Malato Rodriguez S., Agüera López A., Acevedo Merino A., Lopera A.E.-C., et
341 al., 2019. Oxidation mechanisms of amoxicillin and paracetamol in the photo-Fenton solar process. *Water*
342 *Res.* 156, 232-240.

343 Huang W., Bianco A., Brigante M., Mailhot G., 2018. UVA-UVB activation of hydrogen peroxide and persulfate for
344 advanced oxidation processes: Efficiency, mechanism and effect of various water constituents. *J. Hazard.*
345 *Mater.* 347, 279-287.

346 Huang W., Brigante M., Wu F., Mousty C., Hanna K., Mailhot G., 2013. Assessment of the Fe(III)–EDDS complex in
347 Fenton-like processes: From the radical formation to the degradation of Bisphenol A. *Environ. Sci. Technol.*
348 47, 1952-1959.

349 Jiang M., Lu J., Ji Y., Kong D., 2017. Bicarbonate-activated persulfate oxidation of acetaminophen. *Water Res.* 116,
350 324-331.

351 Kaur B., Kuntus L., Tikker P., Kattel E., Trapido M., Dulova N., 2019. Photo-induced oxidation of ceftriaxone by
352 persulfate in the presence of iron oxides. *Sci. Total Environ.* 676, 165-175.

353 Li R., Zhao C., Yao B., Li D., Yan S., O'Shea K.E., et al., 2016. Photochemical transformation of aminoglycoside
354 antibiotics in simulated natural waters. *Environ. Sci. Technol.* 50, 2921-2930.

355 Nazari R., Rajic L., Xue Y., Zhou W., Alshwabkeh A.N., 2018. Degradation of 4-chlorophenol in aqueous solution by

356 sono-electro-Fenton process. *Int. J. Electrochem. Sci.* 13, 9214-9230.

357 Neta P., Hule R.E., Ross A.B., 1988. Rate constant for reactions of inorganic radicals in aqueous solution. *J. Phys. Chem.*

358 *Ref. Data* 17, 1027-1284.

359 Romero V., Acevedo S., Marco P., Giménez J., Esplugas S., 2016. Enhancement of Fenton and photo-Fenton processes

360 at initial circumneutral pH for the degradation of the β -blocker metoprolol. *Water Res.* 88, 449-457.

361 Stookey L.L., 1970. Ferrozine - a new spectrophotometric reagent for iron. *Anal. Chem.* 42, 779-781.

362 Tanaka T., Kouno I., 2003. Oxidation of tea catechins: Chemical structures and reaction mechanism. *Food Sci. Technol.*

363 *Res.* 9, 128-133.

364 Tian X., Jin H., Nie Y., Zhou Z., Yang C., Li Y., et al., 2017. Heterogeneous Fenton-like degradation of ofloxacin over a

365 wide pH range of 3.6–10.0 over modified mesoporous iron oxide. *Chem. Eng. J.* 328, 397-405.

366 Velo Gala I., López - Peñalver J., Sánchez-Polo M., Rivera-Utrilla J., 2014. Comparative study of oxidative degradation

367 of sodium diatrizoate in aqueous solution by $\text{H}_2\text{O}_2/\text{Fe}^{2+}$, $\text{H}_2\text{O}_2/\text{Fe}^{3+}$, Fe (VI) and UV, $\text{H}_2\text{O}_2/\text{UV}$, $\text{K}_2\text{S}_2\text{O}_8/\text{UV}$.

368 *Chem. Eng. J.* 241, 504-512.

369 Wang X., Dong W., Brigante M., Mailhot G., 2019. Hydroxyl and sulfate radicals activated by Fe(III)-EDDS/UV:

370 Comparison of their degradation efficiencies and influence of critical parameters. *Appl. Catal., B* 245,

371 271-278.

372 Wu T., Wu C., Xiang Y., Huang J., Luan L., Chen S., et al., 2016. Kinetics and mechanism of degradation of chitosan by

373 combining sonolysis with H_2O_2 /ascorbic acid. *RSC Adv.* 6, 76280-76287.

374 Wu Y., Bianco A., Brigante M., Dong W., de Sainte-Claire P., Hanna K., et al., 2015. Sulfate radical photogeneration

375 using Fe-EDDS: Influence of critical parameters and naturally occurring scavengers. *Environ. Sci. Technol.* 49,

376 14343-14349.

377 Yamamoto H., Nakamura Y., Moriguchi S., Nakamura Y., Honda Y., Tamura I., et al., 2009. Persistence and partitioning

378 of eight selected pharmaceuticals in the aquatic environment: Laboratory photolysis, biodegradation, and
379 sorption experiments. *Water Res.* 43, 351-362.

380 Yang H., Xue X., Li H., Apandi S.N., Tay-Chan S.C., Ong S.P., et al., 2018. The relative antioxidant activity and steric
381 structure of green tea catechins - A kinetic approach. *Food Chem.* 257, 399-405.

382

383

384 **Figure captions**

385

386 **Figure 1:** UV-vis spectra of CAT 100 μM , Fe^{3+} 100 μM and CAT + Fe^{3+} (both at 100 μM) in water
387 solution at pH 3.3.

388

389 **Figure 2:** (A) Formation of Fe^{2+} from 100 μM of Fe^{3+} using different CAT concentrations for 1
390 hour. (B) Correlation between ratios $[\text{Fe}^{2+}]/[\text{Fe}_{\text{tot}}]$ and $[\text{CAT}]/[\text{Fe}^{3+}]$. Values are determined after 2
391 min in order to ensure that reduction of Fe^{3+} due to the reactivity of CAT is achieved.

392

393 **Figure 3:** Degradation of ATL (10 μM) using different solution in which 5 μM of CAT are mixed
394 with 50 μM of Fe^{2+} or Fe^{3+} and/or 100 μM of PS at pH = 3.3. Insert: Formation of Fe^{2+} when
395 Fe^{3+} and CAT are mixed in the presence and in the absence PS.

396

397 **Figure 4:** CAT stability (A) by monitoring its degradation under different conditions (10 μM ATL,
398 50 μM Fe^{3+} and 100 μM PS) and (B) by analyzing the pseudo-first order decay of 10 μM ATL using
399 various CAT concentration (from 0 to 25 μM). Insert: corresponding degradation curves of ATL as
400 a function of CAT concentration.

401

402 **Figure 5 :** Effect of UVA radiation on the ATL (10 μM) degradation in different solutions
403 containing 5 μM of CAT, 50 μM of Fe^{3+} and 100 μM of PS at pH 3.3.

404

405 **Figure 6:** Scavenging experiments using 10 mM of 2-Pr ort-BuOH under dark (A) and UVA (B)
406 experiments. 10 μM of ATL are mixed with 5 μM of CAT, 50 μM of Fe^{3+} and 100 μM of PS at pH

407 3.3.

408